IMMUNOMETABOLISM

T cells with dysfunctional mitochondria induce multimorbidity and premature senescence

Gabriela Desdín-Micó[1,2], Gonzalo Soto-Heredero[1,2]*, Juan Francisco Aranda[1,2]*, Jorge Oller[1,2]*, Elisa Carrasco[1,2], Enrique Gabandé-Rodríguez[1,2], Eva Maria Blanco[1,2], Arantzazu Alfranca[3], Lorena Cussó[4,5,6,7], Manuel Desco[4,5,6,7], Borja Ibañez[5,8,9], Arancha R. Gortazar[10], Pablo Fernández-Marcos[11], Maria N. Navarro[2,3], Bruno Hernaez[2], Antonio Alcamí[2], Francesc Baixauli[12]†, María Mittelbrunn[1,2]†‡

The effect of immunometabolism on age-associated diseases remains uncertain. In this work, we show that T cells with dysfunctional mitochondria owing to mitochondrial transcription factor A (TFAM) deficiency act as accelerators of senescence. In mice, these cells instigate multiple aging-related features, including metabolic, cognitive, physical, and cardiovascular alterations, which together result in premature death. T cell metabolic failure induces the accumulation of circulating cytokines, which resembles the chronic inflammation that is characteristic of aging ("inflammaging"). This cytokine storm itself acts as a systemic inducer of senescence. Blocking tumor necrosis factor–α signaling or preventing senescence with nicotinamide adenine dinucleotide precursors partially rescues premature aging in mice with *Tfam*-deficient T cells. Thus, T cells can regulate organismal fitness and life span, which highlights the importance of tight immunometabolic control in both aging and the onset of age-associated diseases.

The emerging field of immunometabolism (*1*–*5*) has expanded therapeutic opportunities for the treatment of not only inflammatory and autoimmune disorders (*6*) but also metabolic diseases and cancer (*7*–*10*). However, the utility of targeting immunometabolism to prevent the onset of age-associated diseases and multimorbidity has not been previously addressed.

An age-related decline in mitochondrial function has been observed in various cells and tissues, including T cells (*11*). To investigate the consequences of T cell metabolic decline in healthy aging, we used $Tfam^{fl/fl}$ $Cd4^{Cre}$ mice. *Tfam* is a nuclear gene that encodes mitochondrial transcription factor A (TFAM), which both stabilizes mitochondrial DNA (mtDNA) and initiates mtDNA replication (*12*). In $Tfam^{fl/fl}$ $Cd4^{Cre}$ mice, *Tfam* is depleted in both CD4 and CD8 T lymphocytes (*13*). T cell *Tfam* deficiency reduced the numbers of total circulating CD4 and CD8 T cells (fig. S1A). Lack of *Tfam* resulted in a sharp decrease in T cell mtDNA content (fig. S1B) and the failure to express key electron transport chain components, which reprogrammed T cell metabolism toward glycolysis (*13*) (Fig. 1, A to C). T cells from young (2-month-old) $Tfam^{fl/fl}$ $Cd4^{Cre}$ mice recapitulated features of the mitochondrial dysfunction that appears in aged (22-month-old) wild-type mice (Fig. 1, A to C). This mitochondrial decline was associated with T helper 1 (T_H1) cell skewing, characterized by higher secretion of inflammatory type 1 cytokines interferon-γ (IFN-γ) and tumor necrosis factor–α (TNF-α), and the increased expression of the T_H1 cell master regulator T-bet (Fig. 1, D and E, and fig. S1C). In addition to this proinflammatory phenotype, young (2-month-old) $Tfam^{fl/fl}$ $Cd4^{Cre}$ mice were immunocompromised to a similar extent as old (22-month-old) wild-type mice. We infected $Tfam^{fl/fl}$ $Cd4^{Cre}$ mice with ectromelia virus (ECTV), a highly virulent mouse poxvirus that causes a disease similar to human smallpox, and compared them with young control or old wild-type mice. Infection with ECTV killed old wild-type mice and young $Tfam^{fl/fl}$ $Cd4^{Cre}$ mice within the first 10 days of infection, whereas all young controls were able to survive this acute infection (Fig. 1F). Thus, *Tfam*-deficient T cells recapitulate the metabolic, phenotypic, and functional features of aged T cells. Seven-month-old $Tfam^{fl/fl}$ $Cd4^{Cre}$ mice exhibited premature inflammaging, with circulating levels of the inflammaging-associated cytokines IL-6, IFN-γ, and TNF-α similar to the levels observed in 22-month-old wild-type mice (Fig. 1G and fig. S1, D and E). In humans, inflammaging predicts susceptibility to cardiovascular diseases, neurodegeneration, frailty, and multimorbidity (*14*–*16*). $Tfam^{fl/fl}$ $Cd4^{Cre}$ mice displayed a prematurely aged appearance from the age of 7 months (Fig. 1H), which progressed to anemia, kyphosis, and low body weight (Fig. 1, I to K, and fig. S1F). An additional indicator of aging in $Tfam^{fl/fl}$ $Cd4^{Cre}$ mice was the significant thinning of hypodermal fat (Fig. 1L). Consistent with a premature aging phenotype, metabolic cage experiments revealed that $Tfam^{fl/fl}$ $Cd4^{Cre}$ mice were less active and slower than controls, despite higher energy expenditure (Fig. 1M and fig. S1G). Notably, mean life span in $Tfam^{fl/fl}$ $Cd4^{Cre}$ mice was half that of controls (483 days versus 984 days) (Fig. 1N). Although *Tfam* deletion in regulatory T cells induces lethal autoimmunity (*17*), $Tfam^{fl/fl}$ $Cd4^{Cre}$ mice showed no differences in serum autoantibody levels (fig. S1H).

To evaluate the potential of $Tfam^{fl/fl}$ $Cd4^{Cre}$ mice as a model of age-related multimorbidity, we analyzed muscular, cardiovascular, and cognitive fitness. Histological analyses of $Tfam^{fl/fl}$ $Cd4^{Cre}$ muscle tissue revealed a reduced fiber diameter (Fig. 2A). Imaging analysis of the gastrocnemius muscle after injection of ^{18}F-fluorodeoxyglucose (^{18}F-FDG) revealed significantly lower glucose uptake in $Tfam^{fl/fl}$ $Cd4^{Cre}$ mice (Fig. 2B), and lower skeletal muscle strength was confirmed by the grip strength test (Fig. 2C). Moreover, $Tfam^{fl/fl}$ $Cd4^{Cre}$ muscle up-regulated the expression of genes encoding the ubiquitin ligases MuRF-1 and Atrogin-1 as well as the expression of inflammatory markers (Fig. 2D and fig. S2A). $Tfam^{fl/fl}$ $Cd4^{Cre}$ mice displayed a marked loss of gonadal white adipose tissue (gWAT) mass and smaller adipocytes (Fig. 2, E and F). These differences were accompanied by elevated expression levels of the adipose triglyceride lipase in gWAT and elevated circulating levels of nonesterified fatty acids, both of which were indicative of lipolysis induction (Fig. 2, G and H). Thus, the loss of T cell immunometabolic control induces sarcopenia and lipolysis. Additionally, $Tfam^{fl/fl}$ $Cd4^{Cre}$ mice showed evidence of cardiac atrophy (Fig. 2I and fig. S2B). Histological and echocardiographic analyses revealed relative reduction in left ventricular thickness, reduced left ventricular diameter and volume, and smaller cardiomyocyte size (Fig. 2J and fig. S2, C to F). These features were accompanied by a higher heart rate (Fig. 2K) and the induction of cardiac stress markers *Foxo3a* and *Nppa* (fig. S2G). $Tfam^{fl/fl}$ $Cd4^{Cre}$ mice displayed diastolic failure, characterized by reduced cardiac output, as well as elevated normalized lung weight with signs of lung congestion, as shown by computed tomography scan (Fig. 2, L and M, and fig. S2H).

[1]Instituto de Investigación Sanitaria Hospital 12 de Octubre (imas12), Madrid, Spain. [2]Departamento de Biología Molecular, Centro de Biología Molecular Severo Ochoa (CBMSO), Consejo Superior de Investigaciones Científicas (CSIC)-Universidad Autónoma de Madrid (UAM), Madrid, Spain. [3]Hospital Universitario de la Princesa, Madrid, Spain. [4]Departamento de Bioingeniería e Ingeniería Aeroespacial, Universidad Carlos III de Madrid, Madrid, Spain. [5]Centro Nacional de Investigaciones Cardiovasculares (CNIC), Madrid, Spain. [6]Instituto de Investigación Sanitaria Gregorio Marañón, Madrid, Spain. [7]Centro de Investigación Biomédica en Red de Salud Mental (CIBERSAM), Madrid, Spain. [8]IIS-Fundación Jiménez Díaz, Madrid, Spain. [9]Centro de Investigación Biomédica en Red, Enfermedades Cardiovasculares (CIBERCV), Madrid, Spain. [10]Bone Physiopathology Laboratory, Applied Molecular Medicine Institute (IMMA), Universidad San Pablo-CEU, Madrid, Spain. [11]Metabolic Syndrome Group - BIOPROMET, Madrid Institute for Advanced Studies - IMDEA Food, CEI UAM +CSIC, Madrid, Spain. [12]Department of Immunometabolism, Max Planck Institute of Immunobiology and Epigenetics, Freiburg, Germany.
*These authors contributed equally to this work.
†These authors contributed equally to this work.
‡Corresponding author. Email: mmittelbrunn@cbm.csic.es

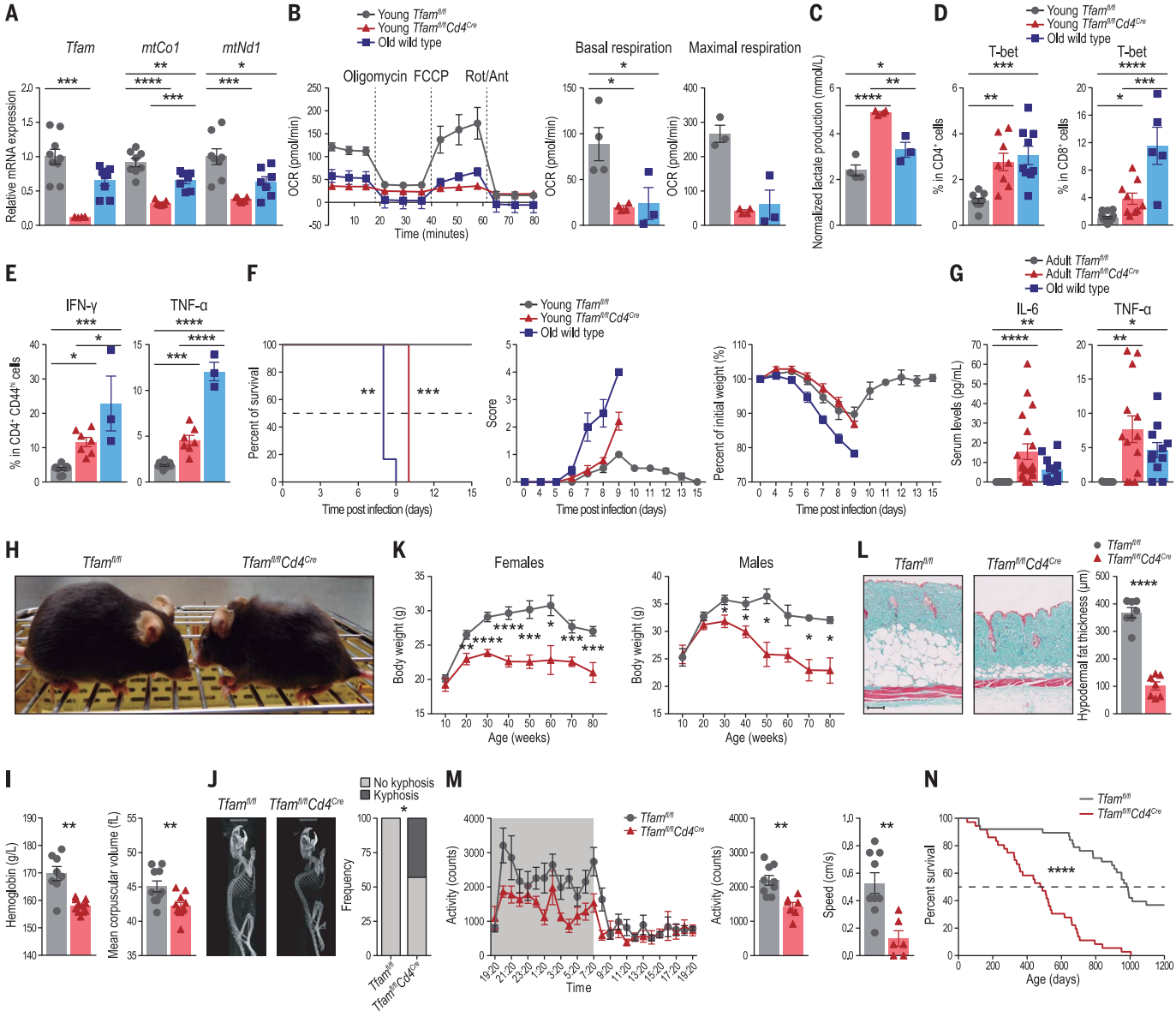

Fig. 1. Mitochondrial dysfunction in T cells causes premature aging. (**A**) *Tfam*, *mtCo1*, and *mtNd1* mRNA levels in peripheral blood CD4$^+$ T cells from young (2-month-old) *Tfam*$^{fl/fl}$ and *Tfam*$^{fl/fl}$ *Cd4*^{Cre} mice and old (22-month-old) wild-type (WT) mice (n = 6 to 9 mice per group). (**B**) (Left) Oxygen consumption rates (OCR) in activated CD4$^+$ T cells from *Tfam*$^{fl/fl}$, *Tfam*$^{fl/fl}$ *Cd4*^{Cre}, and old WT animals. Basal respiration (center) and maximal respiratory capacity (right) are shown (n = 3 to 4). FCCP, carbonyl cyanide-4-(trifluoromethoxy)phenylhydrazone; Rot, rotenone; Ant, antimycin A. (**C**) Lactate content in the supernatant of activated CD4$^+$ T cells (n = 3 to 4). (**D**) Percentages of CD4$^+$ (left) and CD8$^+$ (right) T cells positive for the T_H1 cell transcription factor T-bet (n = 5 to 14). (**E**) Percentages of CD4$^+$CD44^{hi} T cells staining positive for intracellular IFN-γ and TNF-α (n = 3 to 9). (**F**) Postinfection survival curves (left) for *Tfam*$^{fl/fl}$, *Tfam*$^{fl/fl}$ *Cd4*^{Cre}, and old WT mice inoculated subcutaneously with ECTV [10^3 plaque-forming units (PFU) per mouse]. ECTV-infected mice were monitored daily for clinical signs of illness (center) and change from initial body weight (right). Signs of illness are expressed as means ± SEM using an individual score ranging from 0 for healthy animals to 4 for severely diseased animals (n = 5 to 7). (**G**) Serum levels of inflammatory cytokines IL-6 and TNF-α detected by multiplex in 7-month-old *Tfam*$^{fl/fl}$ and *Tfam*$^{fl/fl}$ *Cd4*^{Cre} mice and 22-month-old WT mice (n = 10 to 19). (**H**) Representative photograph showing the deteriorated physical appearance of a *Tfam*$^{fl/fl}$ *Cd4*^{Cre} mouse (right) compared with a control littermate (left), both aged 7 months. (**I**) Hematological parameters in *Tfam*$^{fl/fl}$ *Cd4*^{Cre} and *Tfam*$^{fl/fl}$ mice (n = 8 to 11 5-month-old mice). (**J**) Quantification of spine curvature by computed tomography (CT) scans (left) and percentage of mice presenting lordokyphosis (right) in 5-month-old *Tfam*$^{fl/fl}$ *Cd4*^{Cre} mice (n = 7 to 8). (**K**) Body weight evolution in *Tfam*$^{fl/fl}$ and *Tfam*$^{fl/fl}$ *Cd4*^{Cre} female (left) and male (right) mice (n = 8 to 20). (**L**) Representative skin sections stained with Masson trichrome (left) and quantification of hypodermal fat thickness (right). At least 10 measurements were performed per animal. The graph shows mean values for n = 7 mice at 7 months of age. Scale bar, 100 μm. (**M**) Activity time course over a 24-hour cycle (left) and mean dark period activity (center) and speed (right) assessed in metabolic cages (n = 6 to 9 7-month-old mice). Bar graphs correspond to the dark (active) period. (**N**) Kaplan-Meier survival curves for *Tfam*$^{fl/fl}$ and *Tfam*$^{fl/fl}$ *Cd4*^{Cre} mice (n = 36 to 38 mice, including males and females). Dots in all panels represent individual sample data. Data are presented as means ± SEM. Statistical analysis was by one-way analysis of variance (ANOVA) with post hoc Tukey's correction [(A), *mtCo1* and *mtNd1*; (C), (D), and (G), TNF-α]; Kruskal-Wallis H test with post hoc Dunn's correction [(A), *Tfam*; (B) and (G), IL-6]; unpaired Student's t test [(I), MCV; (J), (K), and (M)]; or unpaired Welch's t test [(L) and (I), hemoglobin]. *P < 0.05; **P < 0.01; ***P < 0.001; ****P < 0.0001. Survival curve data were analyzed by log-rank (Mantel-Cox test) [(F) and (N)]. For the ECTV experiment, data correspond to one of two representative experiments.

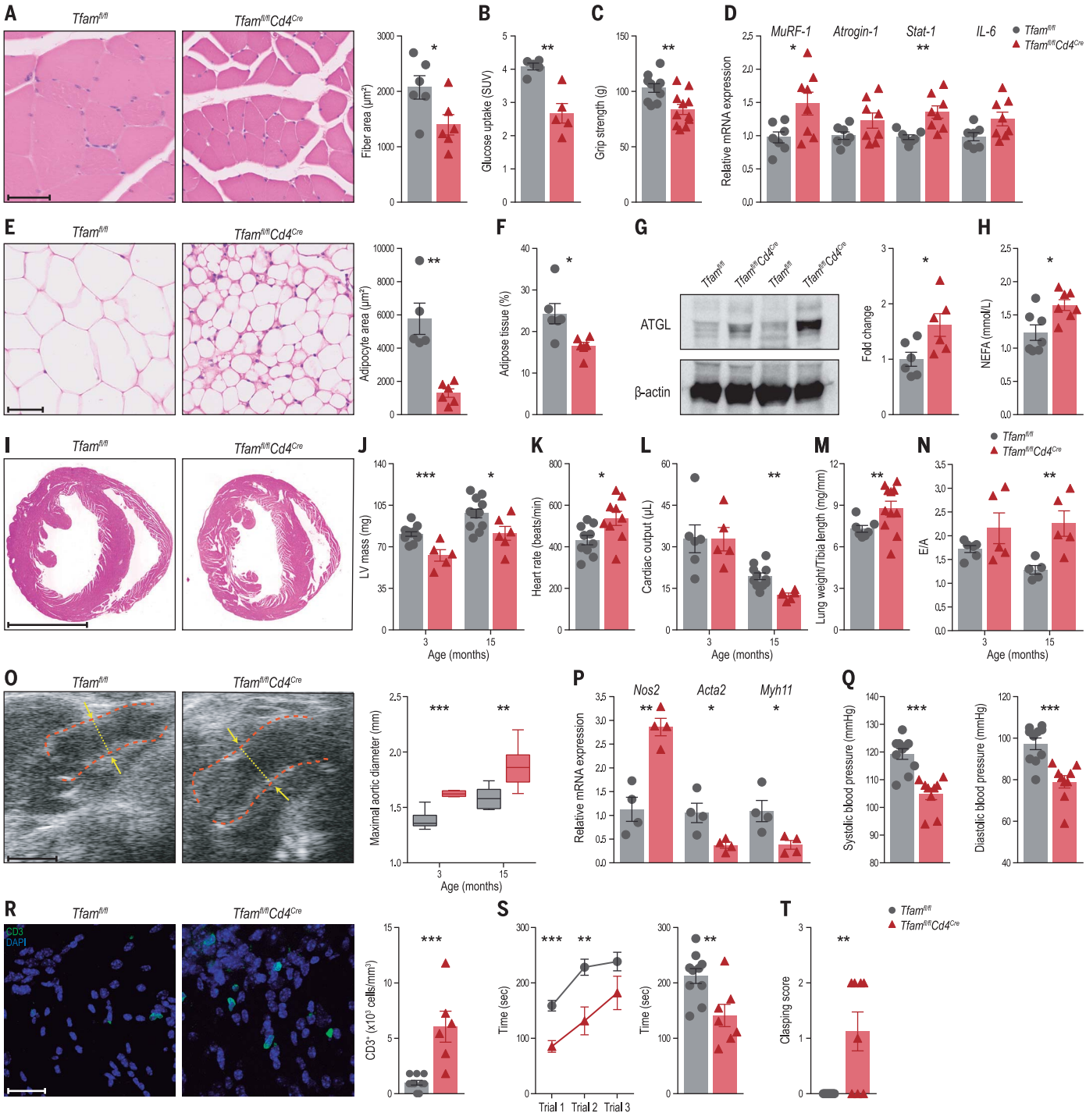

Fig. 2. *Tfam*$^{fl/fl}$ *Cd4*^{Cre} mice develop age-associated multimorbidity. (**A**) Representative hematoxylin and eosin (H&E)–stained sections of the gastrocnemius muscle (left; scale bar, 50 μm) and quantification of myofiber cross-sectional area (right). At least 10 measurements were performed per animal. The graph shows mean fiber area for n = 6 animals per group (7-month-old mice). (**B**) In vivo positron emission tomography and CT analysis of skeletal muscle glucose uptake. Data are means ± SEM of ^{18}F-FDG activity (n = 5 4-month-old mice). SUV, standard uptake value. (**C**) Forelimb grip strength analysis (n = 10 to 11 7-month-old mice). (**D**) Relative mRNA levels of genes related to muscle proteolysis [*Murf1* and Atrogin-1 (*Fbxo32*)] and inflammation (*Stat1* and *Il6*) (n = 7 to 8 7-month-old mice). (**E**) Representative H&E-stained sections of gWAT from *Tfam*$^{fl/fl}$ *Cd4*^{Cre} and *Tfam*$^{fl/fl}$ mice (left; scale bar, 50 μm). The graph (right) shows mean estimated adipocyte surface area. Ten measurements were performed per animal (n = 5 to 6 animals, 7-month-old mice). (**F**) Percentage of adipose tissue determined by quantitative magnetic resonance imaging in *Tfam*$^{fl/fl}$ *Cd4*^{Cre} and *Tfam*$^{fl/fl}$ mice (n = 6 7-month-old mice). (**G**) Immunoblot (left) and densitometry analysis (right) of adipose triglyceride lipase (ATGL) protein expression in gWAT isolated from *Tfam*$^{fl/fl}$ *CD4*^{Cre} mice and control littermates (n = 6 7-month-old mice). (**H**) Plasma nonesterified fatty acids (NEFA) (n = 7 4-month-old mice). (**I**) Representative H&E-stained heart sections from 15-month-old *Tfam*$^{fl/fl}$ *Cd4*^{Cre} and *Tfam*$^{fl/fl}$ mice. Scale bar, 2.5 mm. (continued on next page)

(**J**) Echocardiography measurements of left ventricular (LV) mass in 3- and 15-month-old *Tfam*$^{fl/fl}$ and *Tfam*$^{fl/fl}$ *Cd4*^{Cre} mice (n = 5 to 12). (**K**) Heart rate in 3-month-old *Tfam*$^{fl/fl}$ *Cd4*^{Cre} mice and control littermates (n = 9 to 10). (**L**) Cardiac output in 3- and 15-month-old *Tfam*$^{fl/fl}$ and *Tfam*$^{fl/fl}$ *Cd4*^{Cre} mice (n = 5 to 11). (**M**) Lung weight normalized to tibia length in *Tfam*$^{fl/fl}$ and *Tfam*$^{fl/fl}$ *Cd4*^{Cre} mice (n = 7 to 11 7-month-old mice). (**N**) Mitral flow pattern on echocardiography in 3- and 15-month-old *Tfam*$^{fl/fl}$ and *Tfam*$^{fl/fl}$ *Cd4*^{Cre} mice (n = 5 to 6). E/A, E wave/A wave ratio. (**O**) Representative ultrasound images depicting maximal ascending aorta diameters in 15-month-old *Tfam*$^{fl/fl}$ and *Tfam*$^{fl/fl}$ *Cd4*^{Cre} mice (left; scale bar, 1 mm) and quantification of maximal aortic diameter in 3- and 15-month-old *Tfam*$^{fl/fl}$ and *Tfam*$^{fl/fl}$ *Cd4*^{Cre} mice (right) (n = 6 to 8). Maximal aortic diameter is presented in box-and-whisker plots showing the median, maximal, and minimal values and 75th and 25th percentiles. (**P**) Real-time quantitative polymerase chain reaction (RT-qPCR) analysis of *Nos2*, *Acta2*, and *Myh11* mRNA expression levels in aortic samples from 7-month-old *Tfam*$^{fl/fl}$ and *Tfam*$^{fl/fl}$ *Cd4*^{Cre} mice (n = 4). (**Q**) Systolic and diastolic blood pressure in 3-month-old *Tfam*$^{fl/fl}$ and *Tfam*$^{fl/fl}$ *Cd4*^{Cre} mice (n = 9 to 10). (**R**) Representative CD3-stained brain (fornix) sections from 15-month-old *Tfam*$^{fl/fl}$ and *Tfam*$^{fl/fl}$ *Cd4*^{Cre} mice (left; scale bar, 25 μm) and quantification of CD3 positive cell density (right) (n = 6 to 10). DAPI, 4′,6-diamidino-2-phenylindole. (**S**) Rotarod test performance by *Tfam*$^{fl/fl}$ and *Tfam*$^{fl/fl}$ *Cd4*^{Cre} mice, expressed as the mean time spent on the rotating rod in each of three trials (left) and in all trials combined (right) (n = 7 to 10 12-month-old mice). (**T**) Maximum clasping score per 30-s test (n = 8 to 9 12-month-old mice). Dots in all panels represent individual sample data. Data are presented as means ± SEM. Statistical analysis was by unpaired Student's t test [(A) to (C) and (D), *Murf1*, *Fbxo32*, and *Il6*; (F) to (L), (N), and (O), 15 months; (P) and (Q), diastolic pressure; and (S)]; unpaired Welch's t test [(D), *Stat1*; (M), (N), and (O), 3 months]; or nonparametric Mann-Whitney U test [(Q), systolic pressure; (R) and (T)]. $^*P < 0.05$; $^{**}P < 0.01$; $^{***}P < 0.001$; $^{****}P < 0.0001$.

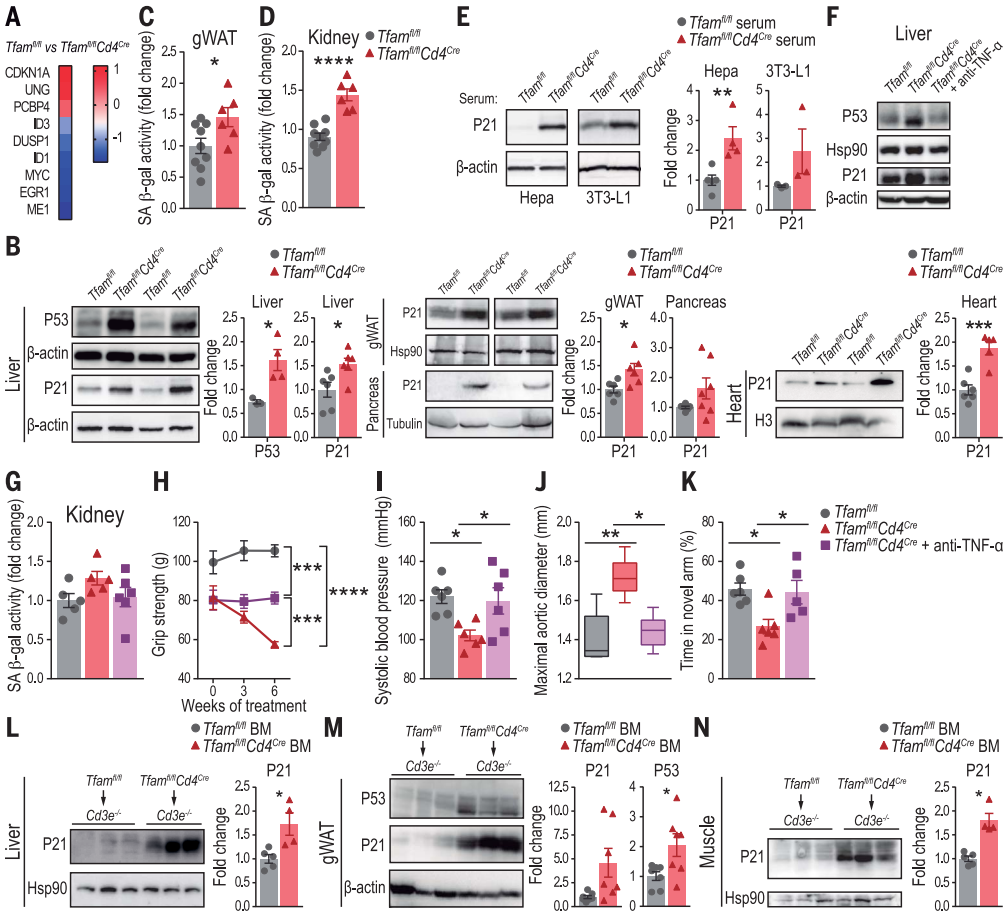

Fig. 3. Inflammaging induces senescence in distal tissues of *Tfam*$^{fl/fl}$ *Cd4*^{Cre} mice. (**A**) Heatmap of senescence gene expression changes comparing livers from *Tfam*$^{fl/fl}$ *Cd4*^{Cre} mice with those from control littermates. (**B**) Representative immunoblot (left) and quantification (right) of p21 and p53 protein expression in the liver, heart, gWAT, and pancreas from *Tfam*$^{fl/fl}$ *Cd4*^{Cre} and *Tfam*$^{fl/fl}$ mice. Loading controls were β-actin, H3, Hsp90, or α-tubulin (n = 4 to 7 7-month-old mice). (**C**) Quantitative measurements of senescence-associated β-galactosidase (SA β-gal) activity in gWAT lysates by colorimetric assay (n = 6 to 9 9-month-old mice). (**D**) Quantitative measurements of SA β-gal activity in kidney lysates by colorimetric assay (n = 6 to 9 12-month-old mice). (**E**) Immunoblot (left) and densitometry analysis (right) of p21 expression in immortalized mouse hepatocytes (Hepa) and 3T3-L1 cells cultured for 7 days in the presence of *Tfam*$^{fl/fl}$ or *Tfam*$^{fl/fl}$ *Cd4*^{Cre} serum from 7-month-old mice. β-actin was used as a loading control (n = 4 to 6). Blots are representative of three (3T3-L1) or four (hepatocytes) experiments using pooled sera from three animals. (**F**) Representative immunoblot analysis of senescence markers in the liver from control *Tfam*$^{fl/fl}$ and *Tfam*$^{fl/fl}$ *Cd4*^{Cre} mice with or without treatment with anti–TNF-α (etanercept) (n = 6, 10 weeks of treatment starting from 4 months of age). (**G**) SA β-gal activity measured by a colorimetric assay in kidney lysates (n = 6, 10 weeks of treatment). (**H**) Time course of forelimb strength during anti–TNF-α treatment. (**I**) Systolic blood pressure after 7 weeks of anti–TNF-α treatment (n = 6). (**J**) Maximal ascending aorta diameter in response to anti–TNF-α treatment (n = 6, 8 weeks of treatment). Maximal aortic diameter is presented in box-and-whisker plots showing maximal and minimal values and 75th and 25th percentiles. (**K**) Y-maze analysis in *Tfam*$^{fl/fl}$ *Cd4*^{Cre} mice treated with anti–TNF-α and corresponding controls (n = 6, 8 weeks of treatment). (**L** to **N**) Immunoblot (left) and densitometry analysis (right) of p21 or p53 expression in liver (L), gWAT (M), and tibialis muscle (N) from *Cd3e*$^{-/-}$ mice 16 weeks after reconstitution with BM from *Tfam*$^{fl/fl}$ *Cd4*^{Cre} or *Tfam*$^{fl/fl}$ mice (n = 4 to 6 per group). Dots in all panels represent individual sample data. Data are presented as means ± SEM. Statistical analysis was by one-way ANOVA with post hoc Tukey's correction [(G), (I), and (K)]; Kruskal-Wallis test with post hoc Dunn's correction (J); two-way ANOVA with post hoc Tukey's correction (H); unpaired Student's t test [(B), (C), (D), (E), (L), and (M)]; or nonparametric Mann-Whitney U test (N). $^*P < 0.05$; $^{**}P < 0.01$; $^{***}P < 0.001$; $^{****}P < 0.0001$.

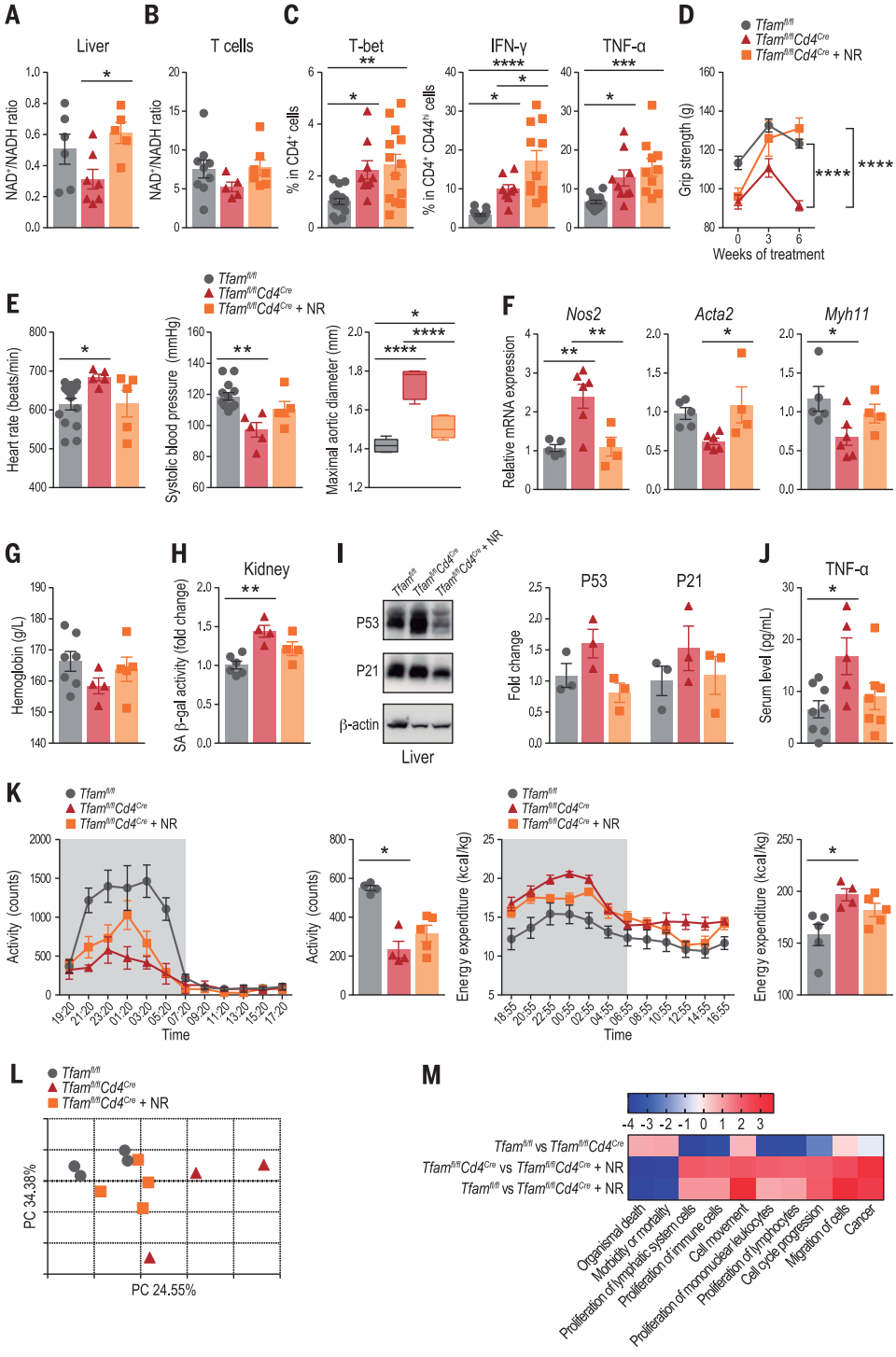

Fig. 4. NR treatment rescues the multimorbidity syndrome. (**A** and **B**) NAD^+/NADH ratio in liver lysates (A) and in isolated $CD4^+$ T cells (B) from untreated *Tfam*$^{fl/fl}$, *Tfam*$^{fl/fl}$ *Cd4*^{Cre}, and NR-treated *Tfam*$^{fl/fl}$ *Cd4*^{Cre} mice (n = 5 to 9 per group, 10-week treatment starting from 4 months of age). (**C**) Flow cytometry analysis of intracellular T-bet (left), IFN-γ (center), and TNF-α (right) in splenic $CD4^+$ T cells (n = 8 to 17 mice). (**D**) Effect of NR treatment on the evolution of forelimb strength (n = 5 to 11). (**E**) Heart rate (left), systolic blood pressure (center), and ascending aorta (AsAo) maximum diameter (right) obtained from ultrasound images after 8 weeks of NR treatment. Maximal aortic diameter is presented in box-and-whisker plots showing the median and the 25th and 75th percentiles (n = 5 to 14). (**F**) RT-qPCR analysis of *Nos2*, *Acta2*, and *Myh11* mRNA expression in the aorta from untreated *Tfam*$^{fl/fl}$, *Tfam*$^{fl/fl}$ *Cd4*^{Cre}, and NR-treated *Tfam*$^{fl/fl}$ *Cd4*^{Cre} mice (n = 4 to 6). (**G**) Blood hemoglobin levels (n = 4 to 7). (**H**) SA β-gal activity measured by colorimetric assay in kidney lysates (n = 4 to 6). (**I**) Immunoblot (left) and densitometry analysis (right) of p21 and p53 expression in liver lysates from untreated *Tfam*$^{fl/fl}$, *Tfam*$^{fl/fl}$ *Cd4*^{Cre}, and *Tfam*$^{fl/fl}$ *Cd4*^{Cre} mice treated with NR for 10 weeks (n = 3 to 4). β-actin was used as a loading control. (**J**) Circulating TNF-α determined by multiplex analysis in serum from untreated *Tfam*$^{fl/fl}$, *Tfam*$^{fl/fl}$ *Cd4*^{Cre}, and NR-treated *Tfam*$^{fl/fl}$ *Cd4*^{Cre} mice (n = 5 to 8). (**K**) Activity (left) and energy expenditure (right) monitored over a 24-hour cycle in metabolic cages (n = 4 to 5). (**L**) Principal components (PC) analysis of transcriptomics in liver samples from untreated *Tfam*$^{fl/fl}$, *Tfam*$^{fl/fl}$ *Cd4*^{Cre}, and *Tfam*$^{fl/fl}$ *Cd4*^{Cre} mice treated with NR for 10 weeks (n = 3 to 4). (**M**) IPA heatmap showing transcriptionally altered cellular pathways. Dots in all panels represent individual sample data. Data are presented as means ± SEM. Statistical analysis was by one-way ANOVA with post hoc Tukey's correction [(A) to (C) and (E), maximal aortic diameter; (G), (H), and (I), p21; (J) and (K), energy expenditure]; Kruskal-Wallis H test with post hoc Dunn's correction [(E), heart rate and systolic blood pressure; (F) and (I), p53; and (K), activity]; or two-way ANOVA with correction post hoc Tukey's correction (D). $^*P < 0.05$; $^{**}P < 0.01$; $^{***}P < 0.001$; $^{****}P < 0.0001$.

Diastolic dysfunction was also evident from left ventricular relaxation defects detected in the mitral flow pattern (Fig. 2N). *Tfam*$^{fl/fl}$ *Cd4*^{Cre} mice developed an age-dependent aortic dilation (Fig. 2O), which is correlated with increased mRNA expression of inducible nitric oxide synthase (*Nos2*), decreased mRNA expression of the contractile markers smooth muscle actin (*Acta2*) and smooth muscle–specific myosin heavy chain (*Myh11*), and decreased blood pressure (Fig. 2, P and Q). Consistent with these findings, 77% of *Tfam*$^{fl/fl}$ *Cd4*^{Cre} mice exhibited aortic regurgitation compared with 16% of controls. Histological analysis of the aortas allowed us to identify aortic dissections associated with inflammatory foci in 50% of *Tfam*$^{fl/fl}$ *Cd4*^{Cre} animals (fig. S2I). Thus, *Tfam*$^{fl/fl}$ *Cd4*^{Cre} mice appear to develop cardiac atrophy, overt heart failure, and severe cardiovascular alterations, all of which can precipitate death. *Tfam*$^{fl/fl}$ *Cd4*^{Cre} mice also showed signs of neurological disability, including an influx of T cells in the fornix region of the brain and defects in motor coordination in both the rotarod and the tail suspension tests (Fig. 2, R to T). Together, these data support a role for T cells beyond host defense (*18*, *19*) and indicate that the metabolic fitness of T cells is critical for organismal homeostasis.

To verify whether this multimorbidity phenotype was caused by a mitochondrial failure in T cells, we used an alternative approach to delete *Tfam* in T cells. We generated *Tfam*$^{fl/fl}$ *Lck*^{Cre} mice, in which Cre recombinase is expressed under the control of the lymphocyte protein tyrosine kinase (*Lck*) promoter. *Tfam*$^{fl/fl}$ *Lck*^{Cre} mice presented comparable metabolic and functional alterations in T cells and similar premature age-associated multimorbidity to those observed in *Tfam*$^{fl/fl}$ *Cd4*^{Cre} mice (fig. S3). To identify the molecular mechanism by which T cell metabolic failure drives organismal frailty and multimorbidity, we performed liver transcriptomics. *Tfam*$^{fl/fl}$ *Cd4*^{Cre} livers showed significant up-regulation of genes associated with senescence (fig. S4A). One of the most up-regulated of these transcripts was *Cdkn1a*, which encodes the cyclin inhibitor p21 (*Q* value = 0.003) (Fig. 3A). *Tfam*$^{fl/fl}$ *Cd4*^{Cre} mice showed elevated protein levels of senescence markers p21$^{Waf/Cip1}$ and p53 in the liver. p21 was also elevated in the heart, gWAT, and pancreas (Fig. 3B). Additionally, the activity of senescence-associated β-galactosidase was higher in *Tfam*$^{fl/fl}$ *Cd4*^{Cre} gWATs and kidneys than in those of controls (Fig. 3, C and D, and fig. S4, B and C). Analysis of *Tfam*$^{fl/fl}$ *Lck*^{Cre} mice confirmed senescence induction in various tissues (fig. S3M).

Because the in vitro incubation of cancer cells with the type 1 cytokines has been shown to induce senescence (*20*), we hypothesized that the type 1 cytokines present in *Tfam*$^{fl/fl}$ *Cd4*^{Cre} mice drive systemic senescence. Incubation of mouse cells with *Tfam*$^{fl/fl}$ *Cd4*^{Cre} serum or TNF-α was sufficient to increase p21$^{Waf/Cip1}$ levels in hepatocytes and preadipocytes, which supports the argument that inflammatory mediators induce senescence and premature aging (Fig. 3E and fig. S4D). To dissect the contribution of TNF-α to the multimorbidity phenotype, we treated *Tfam*$^{fl/fl}$ *Cd4*^{Cre} mice with the TNF-α inhibitor etanercept. Blocking TNF-α prevented systemic senescence (Fig. 3, F and G) and muscle, cardiovascular, and cognitive alterations (Fig. 3, H to K). Bone marrow (BM) transplantation from *Tfam*$^{fl/fl}$ *Cd4*^{Cre} mice into T cell–deficient (*Cd3e*$^{-/-}$) mice (fig. S5, A and B) recapitulated the type 1 cytokine storm observed in *Tfam*$^{fl/fl}$ *Cd4*^{Cre} mice (fig. S5, C to E) and signs of senescence in multiple tissues (Fig. 3, L to N). *Cd3e*$^{-/-}$ mice reconstituted with *Tfam*$^{fl/fl}$ *Cd4*^{Cre} BM, but not with control BM, developed a prematurely aged appearance after 16 weeks (fig. S5F) and reproduced the multimorbidity phenotype (fig. S5, G to J). Thus, T cells with mitochondrial dysfunction are able to induce systemic senescence in peripheral tissues by means of a type 1 cytokine storm.

Notably, the senescence observed in *Tfam*$^{fl/fl}$ *Cd4*^{Cre} mice was accompanied by a low ratio of oxidized nicotinamide adenine dinucleotide (NAD^+) to reduced nicotinamide adenine dinucleotide (NADH) in peripheral tissues (Fig. 4A and fig. S6A). This was consistent with the reported decline in NAD^+ levels during aging (*21*). NAD^+ is a metabolic cofactor with a critical role in mitochondrial function, and restoring NAD^+ levels confers protection against age-associated diseases (*21*–*25*). Recent data suggest that supplementation with the NAD^+ precursor nicotinamide riboside (NR) reduces inflammaging in the elderly (*26*). Accordingly, we observed that NR decreased the serum levels of TNF-α in aged mice (fig. S6B). To test whether NAD^+-boosting strategies could prevent tissue damage caused by inflammaging, we treated *Tfam*$^{fl/fl}$ *Cd4*^{Cre} mice with NR for 10 weeks to restore the NAD^+/NADH ratio (Fig. 4, A and B). Although NR neither prevented weight loss nor reversed the T_H1 cell phenotype (Fig. 4C), it successfully prevented skeletal muscle wasting and anemia. Furthermore, most of the cardiovascular alterations found in *Tfam*$^{fl/fl}$ *Cd4*^{Cre} mice were also prevented (Fig. 4, D to G). NR treatment also increased physical activity levels of *Tfam*$^{fl/fl}$ *Cd4*^{Cre} mice and prevented tissue senescence and inflammation (Fig. 4, H to K, and fig. S6C). Finally, a principal components analysis of liver transcriptomics classified *Tfam*$^{fl/fl}$ *Cd4*^{Cre} mice treated with NR closer to controls than to untreated *Tfam*$^{fl/fl}$ *Cd4*^{Cre} mice (Fig. 4L). Ingenuity pathway analysis (IPA) linked NR treatment to pathways associated with inflammation, morbidity, and mortality (Fig. 4M and table S1). Thus, NR can prevent transcriptional changes related to aging in *Tfam*$^{fl/fl}$ *Cd4*^{Cre} mice.

With the continuous extension of life expectancy, there is an urgent need to understand the common molecular pathways by which aging results in a progressively higher susceptibility to diseases (*27*). Our results indicate that metabolic changes in the immune system promote age-related deterioration in other tissues, which leads to multimorbidity and premature death. Dysregulated T cell metabolism triggers a type 1 cytokine storm that induces senescence in several tissues. Furthermore, we have used this model of multimorbidity and premature aging to test for drugs that can delay aging signs. We found that NAD^+ precursors can prevent the tissue damage associated with sustained inflammation, which supports their potential for preventing age-associated multimorbidity. Further investigation is needed to understand whether targeting senescence or boosting NAD^+ levels could have beneficial effects beyond age-associated diseases in patients with cachexia or cytokine-release syndrome. Our results place immunometabolism at the crossroads of inflammation, senescence, and aging, thereby highlighting its potential as a therapeutic target for delaying aging and aging-associated diseases.

REFERENCE AND NOTES

1. T. N. Tarasenko *et al*., *Cell Metab.* **25**, 1254–1268.e7 (2017).
2. S. E. Weinberg *et al*., *Nature* **565**, 495–499 (2019).
3. L. A. Sena *et al*., *Immunity* **38**, 225–236 (2013).
4. E. L. Pearce *et al*., *Nature* **460**, 103–107 (2009).
5. E. L. Mills, B. Kelly, L. A. J. O'Neill, *Nat. Immunol.* **18**, 488–498 (2017).
6. J. P. Rhoads, A. S. Major, J. C. Rathmell, *Nat. Rev. Rheumatol.* **13**, 313–320 (2017).
7. C. H. Chang, E. L. Pearce, *Nat. Immunol.* **17**, 364–368 (2016).
8. L. Li *et al*., *Cell Metab.* **29**, 103–123.e5 (2019).
9. G. S. Hotamisligil, *Immunity* **47**, 406–420 (2017).
10. A. Wang, H. H. Luan, R. Medzhitov, *Science* **363**, eaar3932 (2019).
11. N. Ron-Harel *et al*., *Proc. Natl. Acad. Sci. U.S.A.* **115**, 13347–13352 (2018).
12. M. I. Ekstrand *et al*., *Hum. Mol. Genet.* **13**, 935–944 (2004).
13. F. Baixauli *et al*., *Cell Metab.* **22**, 485–498 (2015).
14. L. Ferrucci, E. Fabbri, *Nat. Rev. Cardiol.* **15**, 505–522 (2018).
15. C. Franceschi, P. Garagnani, P. Parini, C. Giuliani, A. Santoro, *Nat. Rev. Endocrinol.* **14**, 576–590 (2018).
16. D. Furman *et al*., *Nat. Med.* **25**, 1822–1832 (2019).
17. N. M. Chapman *et al*., *Nat. Commun.* **9**, 2095 (2018).
18. S. He *et al*., *Nature* **566**, 115–119 (2019).
19. L. C. Rankin, D. Artis, *Cell* **173**, 554–567 (2018).
20. H. Braumüller *et al*., *Nature* **494**, 361–365 (2013).
21. A. P. Gomes *et al*., *Cell* **155**, 1624–1638 (2013).
22. E. Verdin, *Science* **350**, 1208–1213 (2015).
23. H. Zhang *et al*., *Science* **352**, 1436–1443 (2016).
24. E. Katsyuba *et al*., *Nature* **563**, 354–359 (2018).
25. S. J. Mitchell *et al*., *Cell Metab.* **27**, 667–676.e4 (2018).
26. Y. S. Elhassan *et al*., *Cell Rep.* **28**, 1717–1728.e6 (2019).
27. I. Bellantuono, *Nature* **554**, 293–295 (2018).

ACKNOWLEDGMENTS

We thank N. G. Larsson for *Tfam*$^{fl/fl}$ mice; R. Tejedor and J. L. de Pablos for technical support; and C. López-Otín, M. Serrano, and B. Alarcón for scientific discussions. We also thank A. de Francisco, Y. Sierra, and M. de la Jara Felipe for their excellent work with animal preparation and imaging protocols and D. Calle for her help with data processing. **Funding:** This study was supported by the Fondo de Investigación Sanitaria del Instituto de Salud Carlos III (PI16/02188 and PI19/00855; and PI16/02110 to B.I.), the European Regional Development Fund (ERDF), and the European Commission through H2020-EU.1.1 and European Research Council grant ERC-2016-StG 715322-EndoMitTalk. This work was partially supported by Comunidad de Madrid (S2017/BMD-3867 RENIM-CM). M.M. is supported by the Miguel Servet Program (CPII 19/00014). G.S.-H. is supported by FPI-UAM, J.O. (FJCI-2017-33855) and E.G.-R. (IJC2018-036850) by Juan de la Cierva, and E.C. by Atracción de Talento Investigador 2017-T2/BMD-5766 (Comunidad de Madrid and UAM). B.I. was supported by ERC research grant ERC-2018-CoG 819775-MATRIX. **Author contributions:** G.D.-M., G.S.-H., J.F.A., J.O., E.C., E.G.-R., M.N.N., L.C., F.B., E.M.B., and B.H. performed experimental work and analyzed the data. B.I., A.Alf., M.D., A.R.G., P.F.-M., and A.Alc. provided technical and scientific support. F.B. and M.M. designed the research. G.D.-M. and M.M. wrote the manuscript. **Competing interests:** The authors declare no competing interests. **Data and materials availability:** All data are presented in the main text or the supplementary materials. The *Tfam*$^{fl/fl}$ mice used in this work were obtained under a material transfer agreement with Max Planck Institute for Biology of Aging.

SUPPLEMENTARY MATERIALS

science.sciencemag.org/content/368/6497/1371/suppl/DC1
Materials and Methods
Figs. S1 to S6
Table S1
References (*28*–*30*)

View/request a protocol for this paper from *Bio-protocol*.

21 February 2019; resubmitted 16 January 2020
Accepted 21 April 2020
Published online 21 May 2020
10.1126/science.aax0860

T cells with dysfunctional mitochondria induce multimorbidity and premature senescence

Gabriela Desdín-Micó, Gonzalo Soto-Heredero, Juan Francisco Aranda, Jorge Oller, Elisa Carrasco, Enrique Gabandé-Rodríguez, Eva Maria Blanco, Arantzazu Alfranca, Lorena Cussó, Manuel Desco, Borja Ibañez, Arancha R. Gortazar, Pablo Fernández-Marcos, Maria N. Navarro, Bruno Hernaez, Antonio Alcamí, Francesc Baixauli and María Mittelbrunn

Science **368** (6497), 1371-1376.
DOI: 10.1126/science.aax0860originally published online May 21, 2020

Inflammaging? Blame T cells!

Mitochondrial dysfunction in various tissues is a prominent characteristic of age-related deterioration, but it is unclear how mitochondrial dysfunction in particular cell types contributes to this process. Desdín-Micó *et al.* generated mice with T cells that were specifically deficient in a mitochondrial DNA–stabilizing protein. These animals exhibited multiple features associated with aging, including neurological, metabolic, muscular, and cardiovascular impairments. The defective T cells initiated an inflammatory program similar to that observed in older animals, a process called "inflammaging." Blocking the cytokine tumor necrosis factor–α or administering precursors of the cofactor nicotinamide adenine dinucleotide restored many of these symptoms of senescence. These findings may potentially inform future therapies for age-associated diseases, as well as cachexia and cytokine-release syndrome.

Science, this issue p. 1371